Desalination and Water Treatment
www.deswater.com

doi: 10.5004/dwt.2021.26665

214 (2021) 252–262
February

Removal of microplastics from industrial wastewater utilizing an ultrafiltration composite membrane rGO/PAN application

Beata Fryczkowska*, Lucyna Przywara

University of Bielsko-Biala, Faculty of Materials, Civil and Environmental Engineering, Institute of Environmental Protection and Engineering, Willowa 2, 43-309 Bielsko-Biala, Poland, emails: bfryczkowska@ath.bielsko.pl (B. Fryczkowska), l.przywara@ath.bielsko.pl (L. Przywara)

Received 30 April 2020; Accepted 14 August 2020

ABSTRACT

Plastic material recycling generates large amounts of industrial wastewater, and for economic reasons, recycled material producers utilize closed systems in which the process water is recirculated multiple times. Wastewater containing microplastics is most often treated with hybrid processes where the final process is generally a membrane process. This study presents the results of composite membranes made of polyacrylonitrile with the addition of reduced graphene oxide (rGO/PAN) utilized for microplastic removal from industrial wastewater. Studies have shown that larger amounts of rGO (from 0.11% to 0.83% w/w) added to the PAN matrix produce a greater number of similar-sized pores (~150 nm), which enables the separation of the colloid formed in the aqueous $FeCl_3$ solution (rejection > 82%) and, more importantly, the microplastics. An important feature of the studied rGO/PAN composite membranes is their anti-fouling properties and the ease of cake layer cleaning, which allows them to be reused. This study has shown that the multi-stage treatment of wastewater containing microplastics can be replaced with a single membrane process using rGO/PAN composite membranes.

Keywords: Microplastics; Composite membrane; Polyacrylonitrile; Reduced graphene oxide; Nanoparticle

1. Introduction

Owing to the rapidly growing plastic production (359 million tons in 2018 [1]) and their processing, storage, and recycling, small plastic fragments, referred to as microplastics (MPs), that directly or indirectly enter into surface water are formed. MPs are generally defined as synthetic polymers with an upper size limit of 5 mm, without a specified lower limit [2,3].

MPs can be removed using physical, chemical, biological, and membrane methods. Physical MP removal methods include sedimentation, flotation, filtration, degasification, and aeration [4]. Among the biological processes, aerobic (activate sludge treatment, tricking filtration, oxidation ponds, lagoons, and aerobic digestion) and anaerobic (anaerobic digestion, septic tanks, and lagoons) methods are the most effective [4]. Biotechnological methods, including the activated sludge method, allow for MP removal efficiencies of 95.16%–98.3% [5,6]. Chemical MP removal methods include chlorination, ozonation, neutralization, coagulation, and adsorption [4]. In addition to these methods, advanced oxidation processes utilizing thermally activated persulfate and Fenton's reagent have been successfully utilized for MP removal [7]. Moreover, widely understood photocatalytic processes [8,9] using zinc oxide nanorods [10,11] and TiO_2 [12] are employed for MP degradation. Other researchers described an MP removal method using electrocoagulation that increased the MP removal efficiency above 90% [13].

* Corresponding author.

Hybrid methods are most often used for MP removal from wastewater. Previous studies suggest that MPs can be removed by coagulation with iron or aluminum salts combined with ultrafiltration (UF) on polyvinylidene membranes [14,15]. Enfrin et al. [16] described the possibility of removing MPs to obtain drinking water utilizing a multi-stage process consisting of the successive stages of coagulation, dissolved air flotation, rapid sand filtration, UF, reverse osmosis, and disinfection.

Selected membrane processes, such as UF, dynamic membrane technology [17], reverse osmosis [18], and membrane bioreactors, are also used to remove MPs from water. Membrane processes account for 13% of all the methods used to remove MPs, of which 5% is via membrane bioreactors [4]. The popular use of membrane bioreactors in membrane processes is owing to their high efficiency (80%–99.9%) [5,6,19].

UF is an economical method to remove various types of contaminants from water or wastewater and the use of UF to remove MPs allows the simultaneous removal of other unnecessary feed ingredients, for example, proteins, fatty acids, bacteria, protozoa, viruses, and suspended solids. UF is often used in conjunction with other methods as the second stage of wastewater or water treatment. A previous study describes the possibility of removing polyethylene particles using UF on commercial polyvinylidene fluoride membranes [15]. In this case, the UF process was preceded by coagulation conducted using polyacrylamide. Other researchers have also used polyvinylidene membranes to remove polyethylene, but the membrane process was preceded by MP coagulation with iron ions [14]. An alternative, one-step polyethylene removal process was proposed by Enfrin et al. [20] using a commercial polysulfone membrane.

This study investigated the use of polyacrylonitrile (PAN)-based composite membranes with the addition of reduced graphene oxide (rGO) to remove MPs from process water and industrial wastewater. Previous research has shown that some rGO/PAN composite membranes are not susceptible to fouling in bovine serum albumin (BSA) separation [21]; therefore, this study attempted to use these membranes to remove polyethylene terephthalate fragments from wastewater. This research has confirmed that rGO/PAN membranes are highly efficient in retaining fragments of solid polymer-derived impurities. A positive characteristic of performing UF under these conditions is the ease and effectiveness of cleaning the membranes. Thus, this study proves the anti-fouling properties of the rGO/PAN composite membranes formed from a small addition of rGO to the PAN matrix.

2. Materials and methods

2.1. Materials

The PAN copolymer utilized in this study (MW = 85,000; 93.9% acrylonitrile, 5.8% methyl acrylate, 0.3% methallyl sulfonate) was purchased from Goodfellow Cambridge Ltd., England. The graphite powder (<20 μm) was purchased from Sigma-Aldrich, Poland. The *N*,*N*-dimethylformamide (DMF), minimum 95% H_2SO_4, 30% H_2O_2, $KMnO_4$, $NaNO_3$, and $FeCl_3$ were purchased from Avantor Performance Materials Poland S.A., Poland.

Graphene oxide was obtained using the modified Hummers method [22], wherein 2 g of graphite powder were added to 46 cm^3 of H_2SO_4, and the resulting suspension was stirred for 30 min in an ice bath. Then, 6 g of $KMnO_4$ was slowly added to the solution to prevent exceeding a temperature of 20°C. The contents of the beaker were then heated to 35°C, stirred for 2 h, and then 92 cm^3 of distilled water was added. To remove the remaining $KMnO_4$, a solution of 80 cm^3 of warm distilled water (60°C) and 50 cm^3 of a 3% H_2O_2 aqueous solution were added. The resulting sample was centrifuged and repeatedly rinsed with distilled water until a pH of 7 was achieved. The next step was the low-temperature thermal reduction of the graphene oxide, which was performed in a nitrogen atmosphere, at a temperature below 300°C, with a heating rate of 30°C/min, and produced a black rGO powder.

2.2. Wastewater containing MPs

The wastewater containing MPs utilized in this study was obtained from a polyethylene terephthalate recycling plant located in Silesian Province of Poland. Two types of wastewater were selected for testing, process water (MP1) and raw wastewater (MP2). MP1, generated during the wastewater treatment processes used by the plant, is mainly composed of water and is recirculated through the production process. MP2, however, is raw wastewater generated in the production process that is not recirculated.

The pH and conductivity (P) of MP1 and MP2 were tested using an Elmetron CPC 511 laboratory pH/P meter. Chemical oxygen demand (COD) was determined using the potassium dichromate method according to PN-74/C-04578.03, PN-ISO 6060:2006. Ammonia nitrogen (NH_4^+), sulfates (SO_4^{2-}), and phosphates (PO_4^{3-}) were determined using ready HACH cuvette test sets on a HACH DR4000 spectrophotometer (according to applicable standards). Dry residue (according to PN-78/C-04541), total dissolved solids (TDS) (according to PN-EN 15216:2010), and total suspended solids (TDS) (according to PN-EN 872:2007+Ap1:2007) were determined using a weight method. The wastewater parameters determined using the mentioned methods for MP1 and MP2 are presented in Table 1.

2.3. Forming PAN and composite rGO/PAN membranes

The membranes were formed by the wet-phase separation/inversion method, as described in a previous study [21]. Initially, a PAN membrane (membrane 0) was obtained from a 12% w/w PAN solution in DMF. The membrane-forming solution concentration selection was determined based on rheological studies that demonstrated that the 12% PAN terpolymer concentration is the most favorable for membrane formation. The polymer was dissolved at 50°C, cooled to room temperature (20°C ± 1°C), and then the PAN solution was poured onto a clean glass plate and spread using a casting knife with a gap width of 0.2 mm. Finally, the polymer film was rapidly coagulated in distilled water at room temperature until the membrane detached from the glass. The precipitated membranes were air-dried by interposing a layer of tissue paper and then loaded onto a glass plate. The solutions necessary for the formation of

the rGO/PAN composite membranes were then prepared. Thus, the required amounts of rGO and DMF were weighed and mixed thoroughly. Then, the required amounts of PAN were added and mixed at 50°C until the polymer was dissolved (Table 2). The resultant rGO/PAN/DMF solution was then poured onto a glass plate and spread using a casting knife with a gap width of 0.2 mm. The film was rapidly coagulated in distilled water at room temperature using the same method as described above for the PAN solution.

The rGO/PAN composite membranes used in this study were selected based on a previous experiment [21], which showed that a positive effect on the membrane separation properties can only be achieved utilizing a small amount of rGO added to the PAN matrix.

2.4. Membrane investigation methods

2.4.1. Physicochemical properties

The membrane's physicochemical properties such as thickness, water sorption, and contact angle are summarised in Table 2, and the results of this study were the same as those in a previous publication [21].

Cross-section and surface porosities and membrane surface pore size were analyzed using a Phenom ProX scanning electron microscopy (SEM) manufactured by Thermo Fisher Scientific (Eindhofen, Netherlands) operating at 10 kV. Liquid nitrogen, which was frozen and then broken, was used to prepare the membrane cross-sections. The diffusion method was utilized to spray apply a 5 nm thick layer of gold to all the membrane samples using a LEICA ACE 200 low vacuum sprayer (Pik Instruments, Piaseczno, Poland). At least three membrane pieces and three images of each piece were measured to obtain one data point. The membrane surface porosity and pore sizes were measured from the surface images using PoroMetric software developed by PhenomWorld. Table 2 presents the results of the cross-section and surface porosity, and Table 3 presents the median values of the selective membrane layer's pore diameter. Fig. 1 presents an example of a cross-section and skin layer image obtained by processing using the PoroMetric software.

2.4.2. Transport properties

The transport properties of the formed membranes were tested using a Millipore Amicon 8400 UF cell with a 350 mL capacity and a 7.6 cm membrane diameter that was equipped with an equalizing tank with an 800 mL capacity. First, the dry membranes were immersed in distilled water for 1 h. Then, they were treated with distilled water for an additional 2 h under a pressure of 0.2 MPa to improve the membrane's stability. UF tests were performed at operational pressures of 0.1, 0.15, and 0.2 MPa. Permeate flux (J_v) was calculated using the following formula:

$$J_v = \frac{V}{A \times t} \tag{1}$$

where J_v is the water flux (L/m² h), V is the permeate volume (L), A is the effective membrane area (m²), and t is the permeation time (h).

Table 3 summarizes the water flux values for the pure PAN membranes (membrane 0) and rGO/PAN composite membranes.

2.4.3. $FeCl_3$ rejection measurements

$FeCl_3$ solution is used in wastewater and industrial waste treatment processes [23]. In this study, it was employed as a foulant to study anti-fouling performance. When this compound is dissolved in water, it is slowly hydrolyzed in three stages. The reactions, in a highly simplified form, are as follows:

Table 1
Composition of wastewater containing MPs

Parameters	MP1	MP2
pH	6.80	10.13
P (μS/cm)	1,794	1,537
COD (mg O_2/L)	850	1,710
TDS (mg/L)	736	630
Ammonia nitrogen (mg/L)	1.75	4.25
Sulfates (mg/L)	65	145
Phosphates (mg/L)	0.5	2.6
Dry residue (mg/L)	1,100	1,500
Total suspended solids (mg/L)	250	600

Table 2
Qualitative composition and physicochemical properties of membranes

Membrane	Concentration of rGO (% w/w)	Concentration of PAN (% w/w)	l (μm)*	U (%)*	α (°)*	P_{cs} (%)	P_s (%)
0	0	100.0	190.1 ± 9.3	249.0 ± 20.6	52.0 ± 2.8	80.93	15.85
A	0.11	99.89	198.8 ± 13.9	259.1 ± 18.4	49.5 ± 2.7	82.77	21.75
B	0.22	99.78	188.9 ± 12.1	261.5 ± 19.9	47.3 ± 4.1	83.15	23.39
C	0.45	99.55	182.5 ± 8.6	289.5 ± 25.5	48.2 ± 2.7	85.23	24.79
D	0.83	99.27	182.8 ± 13.1	325.1 ± 20.9	45.2 ± 2.6	90.51	36.57

*denotes previous publication results [21], l is membrane thickness, U is water sorption, α is contact angle, P_{cs} is cross-section porosity of the membrane, and P_s is the porosity of the selective membrane layer.

Table 3
Water flux and median pore diameter of the membranes

Membrane	J_v (L/m²h)*			Median of pore diameter (nm)
	0.1 (MPa)	0.15 (MPa)	0.20 (MPa)	
0	57.1 ± 5.9	87.7 ± 7.2	127.0 ± 9.8	177
A	42.9 ± 4.1	79.9 ± 6.8	90 ± 8.3	179
B	49.7 ± 5.0	85.9 ± 8.1	121.3 ± 10.5	180
C	67.7 ± 5.3	94.3 ± 9.7	144.2 ± 14.0	182
D	172.6 ± 13.9	220.8 ± 20.1	323.6 ± 24.2	191

*denotes previous publication results [21].

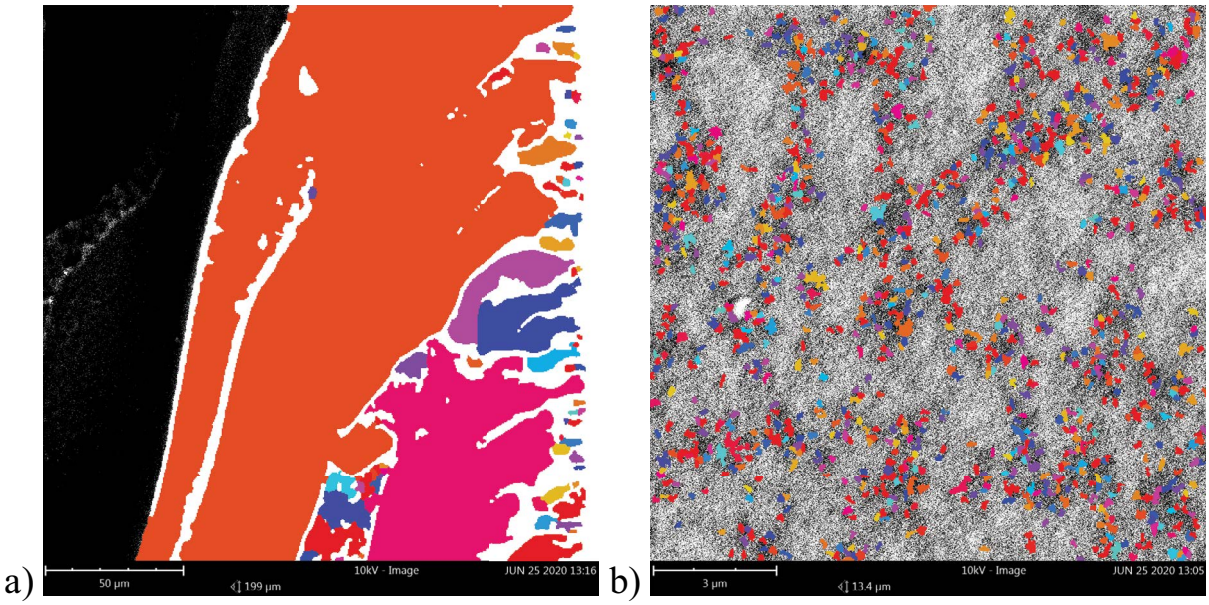

Fig. 1. Pore distribution for membrane 0 obtained using PoroMetric software (a) cross-section (2,000× magnification) and (b) skin layer (20,000× magnification).

$$FeCl_3 + 3H_2O \leftrightarrow Fe(OH)Cl_2 + HCl + 2H_2O \leftrightarrow Fe(OH)_2Cl + 2HCl + H_2O \leftrightarrow Fe(OH)_3 + 3HCl$$

As a result of the dissolution process, an $Fe(OH)_3$ colloid is formed, which is illustrated in Fig. 2.

The particle size of $Fe(OH)_3$ colloid was determined using a Particle Analyzer Litesizer 500 Anton Paar (Graz, Austria). The device's measurement parameters were a measurement cell made of 10 mm × 10 mm polystyrene, a laser with a 658 nm wavelength, a laser spot size of less than 1 mm, a target temperature of 25°C, an equilibration time of 3 min, and a measurement time of 10 s.

The test results showed that an aqueous $FeCl_3$ solution at a concentration of 0.1 g/L has a pH of 2.6 and resulted in a colloid particle size of 181 ± 4 nm.

The PAN and rGO/PAN composite membranes were tested utilizing a 0.1 g/L aqueous $FeCl_3$ solution. First, 400 mL of $FeCl_3$ solution was introduced into a UF cell equipped with the tested membrane and equalizing tank. The permeation process was carried out at an operating pressure of 0.2 MPa and then 40 mL batches of permeate were collected while measuring the permeate outflow time from the test tank. The volumetric permeate flux (J_v) was calculated using Eq. (1).

The $FeCl_3$ concentration in the permeate was indirectly determined by measuring the absorbance of the subsequent solutions using a Perkin Elmer Lambda 35 UV-vis spectrophotometer at a wavelength of 280 nm. Then, the rejection coefficient (R) was calculated using Eq. (2) as follows:

$$R = \left(1 - \frac{C_p}{C_f}\right) \times 100\% \quad (2)$$

where R is the rejection performance of the membrane (%) and C_p and C_f are the $FeCl_3$ concentrations in the permeate and feed solution (g/L), respectively.

2.4.4. Membrane separation of wastewater containing MPs

The ability of rGO/PAN composite membranes to separate BSA, which is described in a previous publication

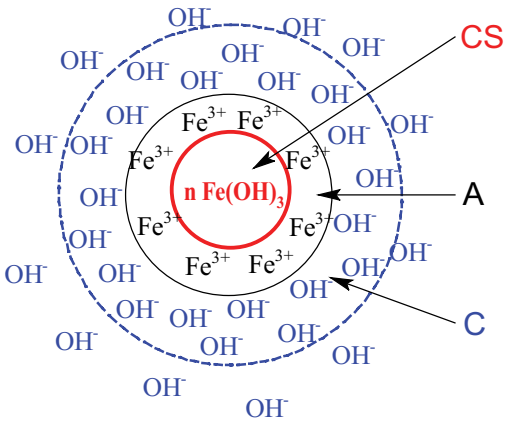

Fig. 2. $Fe(OH)_3$ colloid schematic, where CS is a solid colloid particle, *A* is the absorption layer, and *D* is the diffusion layer.

[21], and their anti-fouling properties with respect to $Fe(OH)_3$, was the impetus for this study to expand the use of rGO/PAN composite membranes. MP removal from water is an interesting and intensively studied topic and this study investigated the possibility of treating industrial wastewater containing MPs (MP1 and MP2) using the rGO/PAN composite membranes produced in this study by the method described in section 2.3 (Forming PAN and composite rGO/PAN membranes).

First, 400 mL of MP1 was introduced into the UF cell equipped with the tested membrane and equalizing tank. The permeation process was carried out at an operating pressure of 0.2 MPa and 40 mL batches of permeate were collected while measuring the permeate outflow time from the test tank. The volumetric permeate flux (J_v MP1) was calculated using Eq. (1). The membrane was washed under running water and then washed three times in a UF cell to remove impurities from the membrane pores. For the first time the membrane was turned over, the selective layer was deposited on the bottom of the membrane, after which it was rinsed for 30 min with distilled water at 0.2 MPa. The membrane was then turned over (selective layer on top), washed under running water, and then washed three times in a UF cell. The membrane was turned over a third time and rinsed again. Finally, the test and equalizing tanks were filled with distilled water and, at a pressure of 0.2 MPa, the transport properties of the tested membrane were checked again, calculating the volumetric permeate flux (J_v1) utilizing Eq. (1). Next, MP2 separation was tested on the same membrane employing the same procedure as that utilized on MP1. In the second stage of separation, the wastewater (J_v MP2) and water (J_v2) fluxes were determined successively after wastewater separation and washing three times, as described in the procedure for MP1.

3. Results and discussion

3.1. General characterization of membranes

The tested membranes were characterized according to thickness, water sorption, porosity, contact angle, water flux, and pore size.

Based on the thickness results (Table 2), all the tested membranes had a similar thickness, ranging from 182.5 to 198.8 μm. Notably, a small addition of rGO (0.11% w/w) causes a slight increase in the rGO/PAN composite membrane thickness compared to the pure PAN membrane (membrane 0). However, subsequent amounts of this nanoadditive cause a slight decrease in the composite membrane thickness relative to membrane 0. The thickness results correlate with the porosity results that were measured from the SEM cross-section microphotographs. All the tested membranes were characterized by high overall porosity (Table 2). The porosity of membrane 0 was 80.93%, and for the rGO/PAN composite membranes (membranes *A*, *B*, *C*, and *D*), the porosity slightly increases to 82.77%, 83.15%, 85.23%, and 90.51%, respectively.

Based on the contact angle results (Table 2), it was observed that the addition of rGO increases the membrane's hydrophilicity and the contact angle decreases from ~52.0° for the pure PAN membrane to ~45.2° for membrane *D*. When analyzing the water sorption results, it can be seen that they are closely related to the porosity, contact angle, and membrane thickness results. Membrane 0 has water sorption of ~249% and the water sorption of the rGO/PAN composite membranes *A*, *B*, *C*, and *D* increases with increasing nanoadditive amounts to ~259.1%, ~261.5%, ~289.5%, and ~325.1%, respectively. Membrane *D*'s high water sorption value is due to its high volume porosity.

Based on the comparison of the rGO/PAN composite membranes' physicochemical properties (Table 2), it was determined that the optimal addition amount of rGO to the PAN matrix is 0.83% w/w, which reduces membrane thickness and contact angle and increases water porosity and sorption.

The most important characteristic determined in later applications was the membrane transport properties at a working pressure of 0.2 MPa (Table 3). Under these conditions, the specific permeate flux values for membranes 0, *A*, *B*, *C*, and *D* were ~127, ~90, ~121, ~144, and ~324 L/m² h, respectively.

The structure of the selective layer, evaluated using SEM microscopy and PoroMetric software, is responsible for the membrane's transport and separation properties.

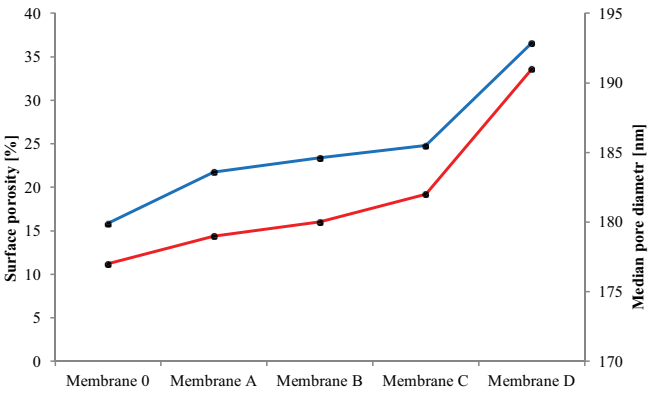

Fig. 3. Membrane surface porosity (blue line) and pore size (red line) measured from the SEM surface images and using PoroMetric software.

The results of the research on the skin layer's porosity and pore size of the tested membranes are summarised in Fig. 3. The porosity of the selective layer and the median pore diameter of membrane 0 were ~16% and 177 nm, respectively. For the rGO/PAN composite membranes, the membrane porosity increased with increasing rGO content. Membranes *A*–*C* had similar porosity values of 22%, ~23%, and ~25%, respectively, and similar median pore diameter values of 179, 180, and 182 nm, respectively. Membrane *D*, which contains 0.83% of rGO, had a much higher porosity (~36%) and median pore diameter (191 nm).

A detailed analysis of the pore size distribution obtained from the PoroMetric software is presented in Fig. 4. Fig. 4 illustrates that, for membrane 0, the selective layer (Fig. 4a) is made of pores with a large size distribution and there are a large number of pores (~90%) ranging in size from ~153 to 203 nm on the surface.

For membranes *A*–*D* (Figs. 4b–e), a minimal pore size distribution was observed; however, the majority of the pores are small, predominantly ~153 nm, and there are a small number of large pores. This phenomenon affects the separation properties of the tested membranes. If the size of

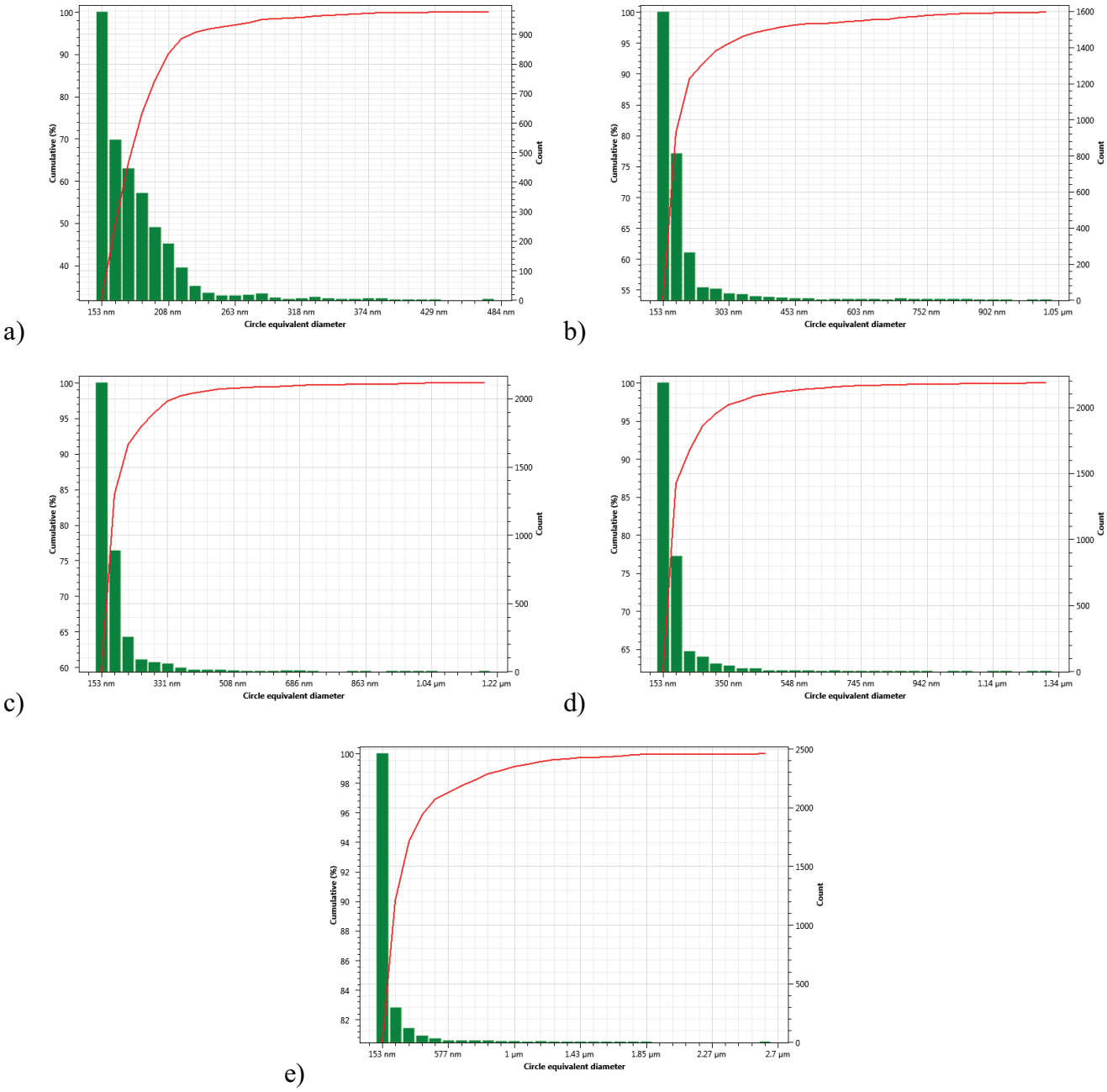

Fig. 4. Pore size scatter plots obtained using PoroMetric software: (a) membrane 0 and (b–e) rGO/PAN composite membranes *A*–*D*, respectively.

the separated particles is larger than the pore size, they will be retained by the membrane; however, if the separated particles are smaller than the pore size, the membrane will not retain them.

3.2. Transport and anti-fouling properties of membranes relative to $FeCl_3$

In this study, the transport and anti-fouling properties of the membranes from pure PAN (membrane 0) and the rGO/PAN composite membranes were examined using an aqueous $FeCl_3$ solution. As observed in the images presented in Fig. 5, membrane 0 was covered with an orange layer (derived from $Fe(OH)_3$), which could not be removed by washing under running water; however, membranes *A*, *B*, and *C* tested under the same conditions only have orange spots and membrane *D* has none. Visual assessment of the rGO/PAN composite membranes may indicate their anti-fouling properties, and the greater the amount of rGO nanoadditive, the more fouling resistant the membrane becomes.

The phenomenon observed in Fig. 5 is due to the slow hydrolysis of $FeCl_3$ to insoluble $Fe(OH)_3$, which forms a colloidal solution and the colloids form agglomerates that can block membrane pores. Their size depends on the solution's pH, temperature, and dissolution time. A previous study reported that in solutions with a concentration of 2 mg/L, the $Fe(OH)_3$ particle sizes range within 30–500 nm [24]. The tests performed in this study prove that the prepared aqueous $FeCl_3$ solution with a pH of 2.6 results in a particle size of 181 ± 4 nm. The obtained result proves that membrane 0 is fouled because its supporting layer is covered with a large number of pores similar to the size of the $Fe(OH)_3$ colloid (Fig. 4a). Although rGO/PAN composite membranes are characterized by a higher surface porosity (Fig. 3), they are predominantly composed of pores that are smaller than the $Fe(OH)_3$ colloid particles (Figs. 4b–e); therefore, the rGO/PAN composite membranes are resistant to fouling.

The transport properties (Fig. 6) showed that the introduction of an aqueous $FeCl_3$ solution onto membrane 0 causes an approximately 5-fold decrease in the permeate flux values from ~127 (Table 3) to ~27 L/m² h. Low permeate flux values are accompanied by a 94% rejection rate, indicating that membrane 0 is fouled under the influence of a $Fe(OH)_3$ colloidal solution.

The rGO/PAN composite membranes are characterized by equally high $Fe(OH)_3$ rejection rates, with values slightly decreasing as the amount of rGO in the PAN matrix increases (Fig. 6). For membranes *A*, *B*, *C*, and *D*, the rejection values were 92%, 86%, 82%, and 82%, respectively. It was also observed that the flow of the $FeCl_3$ solution caused a slight decrease in the permeate flux values. For membrane *A*, the initial volumetric permeate flux value of ~90 L/m² h (Table 3) decreased by approximately 11–80.3 L/m² h after the UF of the $FeCl_3$. The permeate flux values for membranes *B* and *C*, which had a ~5% decrease after the UF of the $FeCl_3$, were 115.3 and 136.2 L/m² h, respectively. However, for membrane *D*, the permeate flux value was 319.6 L/m² h and only decreased by 1.2%. It can be concluded that the rGO/PAN composite membranes have anti-fouling properties under the influence of a $Fe(OH)_3$ colloidal solution.

3.3. Separation properties of the membranes for wastewater containing MPs

The next stage of this study was to investigate the possibility of using rGO/PAN composite membranes to treat wastewater containing MPs. Fig. 7 presents the pictures of the membranes after a two-stage UF process and then being cleaned three times. Based on a visual assessment, it was evident that the pure PAN membrane (membrane 0) was heavily contaminated as its color had changed from white to dark brown. A filtration cake had formed on the surface of membrane 0, which hinders transport through the membrane. The rGO/PAN composite membranes did not have a filtration cake layer, and, as shown in Fig. 7, their color only changed slightly due to the deposited impurities and their selective layer was still visible. The impurity amounts on membranes *A*–*D* are small and decrease in order from *A* to *D*.

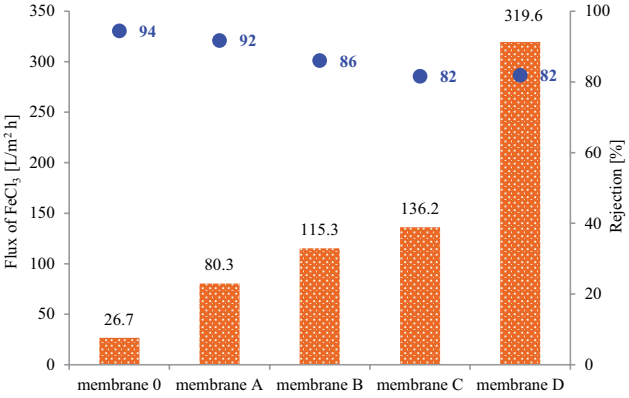

Fig. 6. Volumetric permeate flux of the $FeCl_3$ solution (at an operational pressure of 0.2 MPa) and $FeCl_3$ rejection rates.

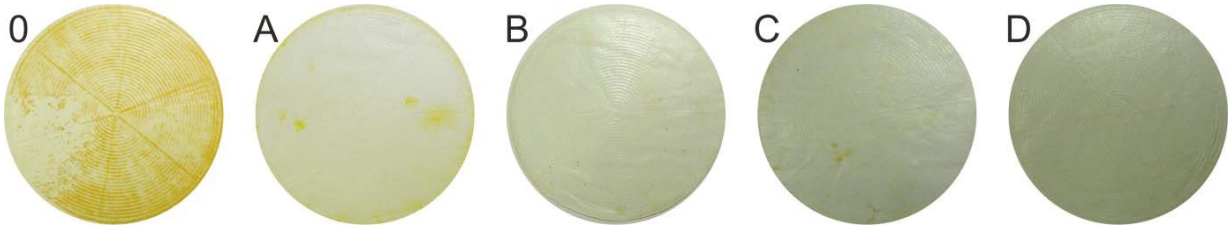

Fig. 5. Images of the membrane 0 (PAN) and rGO/PAN composite membranes (*A*, *B*, *C*, and *D*) after UF using a $FeCl_3$ solution.

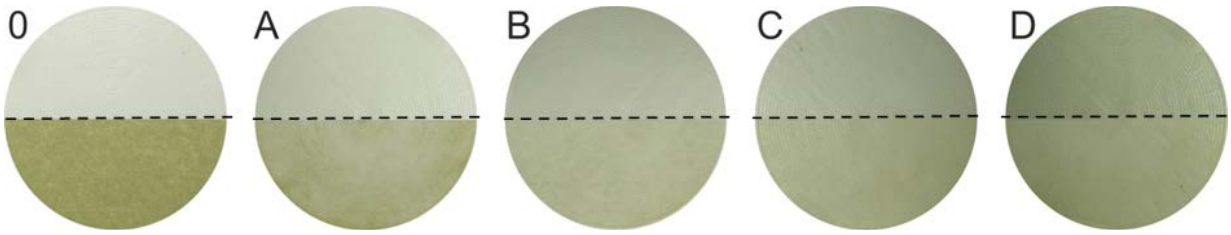

Fig. 7. Photographs of the membranes before (above the dashed line) and after (below the dashed line) two-stage wastewater permeation.

Based on the volumetric permeate flux values (Fig. 8), it was determined that under the influence of wastewater all the membranes experienced fouling. The largest decreases in the permeate flux value were observed for membrane 0 and were 35.5% for J_v MP1 (81.9 L/m² h) and 46% for J_v MP2 (22.1 L/m² h). Cleaning membrane 0 three times after the MP1 separation and three additional times after the MP2 wastewater separation resulted in a water flux of 38.6 L/m² h, which is ~71% of the initial value. Thus, during the separation of wastewater containing MPs, the unmodified membrane is almost completely fouled, which significantly reduces its transport properties. These results confirmed the assumptions drawn from the picture of membrane 0 in Fig. 7.

Based on an analysis of the test results of the rGO/PAN composite membranes (Fig. 8), it can be concluded that they are more resistant to fouling than membrane 0. During UF of MP1, the volumetric permeate flux (J_v MP1) decreased and for membranes *A*, *B*, *C*, and *D*, and the volumetric permeate flux values were 78.7, 103.5, 112.7, and 275.2 L/m² h, respectively. MP2 wastewater separation, which is more polluted than MP1, resulted in a greater decrease in the permeate flux value (J_v MP2) from 19% to 53.2% and the lowest flux values, 69.4 and 151.4 L/m² h, were observed for membranes *C* and *D*, respectively. Cleaning the rGO/PAN composite membranes three times after the MP1 wastewater separation and three additional times after the MP2 wastewater separation resulted in high water flux values. The volumetric permeate flux values for membranes *A*, *B*, *C*, and *D* were 85.0, 116.2, 139.3, and 320.5 L/m² h, respectively. Membrane *D* had the highest flux reduction in wastewater separation and the best transport properties, which might be due to membrane *D* with the highest rGO content of all the composite membranes, thus providing the largest surface porosity (Table 2, Fig. 3).

The tests confirmed that rGO/PAN composite membranes undergo fouling, but in reverse, where the greatest amount of fouling is on membrane *A* and the least amount of fouling is on membrane *D*, which can also be observed in the photographs of these membranes in Fig. 7.

To determine the separation properties of the rGO/PAN composite membranes, the basic parameters of permeates and retentates formed during the UF of MP1 and MP2 were analyzed. The results are summarised in Table 4, which

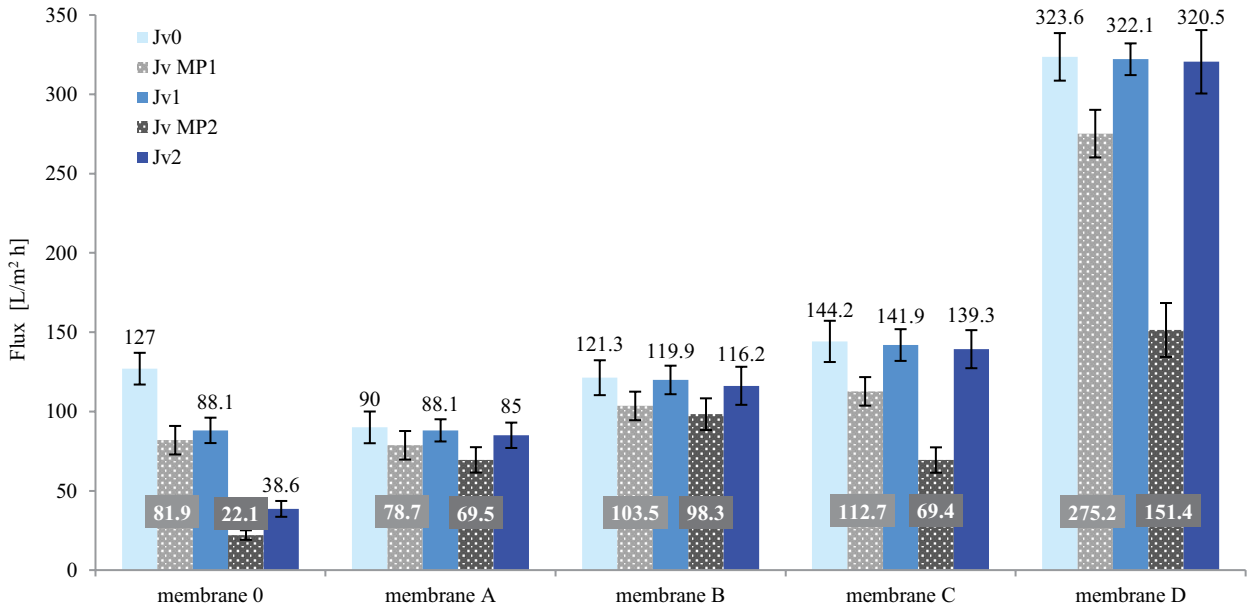

Fig. 8. Volumetric permeate flux values for distilled water (J_v0 – at the beginning of the process, J_v1 – after cleaning MP1 three times, and J_v2 – after cleaning MP2 three times), process water (J_v MP1), and raw wastewater (J_v MP2) at an operational pressure of 0.2 MPa.

Table 4
Physicochemical properties of permeates (*p*) and retentates (*r*) of process water (MP1) and raw wastewater (MP2) obtained in the UF process performed on membranes 0, *A*, *B*, *C*, and *D*

Parameter	pH		P (μS/cm)		COD (mg O_2/L)		TDS (mg/L)		Ammonia nitrogen (mg/L)		Sulfates (mg/L)		Phosphates (mg/L)		Dry residue (mg/L)		Total suspended solids (mg/L)	
								MP1										
Membrane	*p*	*r*	*p*	*r*	*p*	*r*	*p*	*r*	*p*	*r*	*p*	*r*	*p*	*r*	*p*	*r*	*p*	*r*
0	7.60	7.21	1,723	1,783	784	712	707	731	0.01	2.50	45	86.5	0.05	0.50	1,050	1,130	190	210
A	7.66	7.19	1,708	1,774	703	989	701	773	0.16	1.75	47	76	0.07	0.51	1,100	1,150	180	210
B	7.68	7.09	1,711	1,784	695	998	702	764	0.28	1.64	55	70	0.10	0.40	1,105	1,185	175	215
C	7.90	7.06	1,712	1,789	675	1,005	725	731	0.52	1.50	56	52	0.16	0.17	1,150	1,186	174	220
D	8.09	6.97	1,745	1,863	657	1,016	746	728	0.90	1.22	59.5	35	0.45	0.11	1,200	1,190	170	230
								MP2										
0	10.18	10.26	1,448	1,542	1,038	1,381	593	633	0.38	7.50	85	175	0.10	3.67	1,300	1,520	200	400
A	10.05	9.37	1,372	1,501	987	1,414	563	609	0.75	7.30	92.5	144	0.18	2.60	1,310	1,530	185	390
B	9.82	9.53	1,385	1,486	942	1,603	569	614	1.33	6.63	115	138	0.57	2.02	1,350	1,530	180	490
C	9.60	9.54	1,407	1,478	939	1,603	578	599	1.45	6.54	117	130	1.92	0.88	1,380	1,580	180	500
D	9.36	9.70	1,410	1,426	895	2,214	577	606	2.00	5.75	124.5	125	2.30	0.45	1,420	1,590	175	610

indicate that after the process was carried out on the rGO/PAN composite membranes all the MP1 and MP2 parameters changed (Table 1).

Interpretation of the results for complex mixtures such as wastewater is very difficult (Table 4). Previous studies found that the sizes of ammonium cation, phosphate anion, and sulfate anion were ~15, ~20, and ~27 nm, respectively [25]; therefore, the tested rGO composite membranes should not retain these ions. The observed rejection of these ions during UF could be caused by the interaction of the functional groups derived from the polymer from the MPs and membrane components. In addition, ions (cations and anions) passing through the membranes cause equilibrium disturbances; consequently, they can form water-insoluble salts or hydroxides in the permeate and retentate. Based on previous research, tested membranes do not retain salt ions (NaCl and Na_2SO_4).

The P and TDS values are higher for MP1 than for MP2 (Table 4), which might indicate the physicochemical processes of wastewater treatment (MP1) that were performed at the plant. The P and TDS values in the permeates obtained from the rGO/PAN composite membranes slightly increase as the rGO content of the membrane increases (i.e., $A < B < C < D$). For the rGO/PAN composite membranes, when the nanoadditive concentration in the PAN matrix increases ($A > B > C > D$), the COD values in the permeates decrease. Therefore, it can be assumed that the transport of ions to permeates is accompanied by the rejection of organic compounds in the retentates.

The TDS results were unanticipated, showing that impurities smaller than 150 nm (i.e., particle sizes smaller than the smallest membrane pores) could pass through the pores of all the tested membranes. This results in the presence of suspensions in the retentates, which are formed by nanoplastics with a size less than 100 nm [20]; however, the MP1 sample utilized in this study contained virtually no MPs with particle sizes below 5 mm [20]. In contrast, raw sewage, in addition to containing small-sized impurities (below 150 nm), contains solid residues that are too large to be filtered through the membranes and can be observed with the naked eye (Fig. 7).

4. Conclusion

In this study, the applicability of utilizing rGO/PAN composite membranes for the treatment of industrial wastewater containing MPs has been investigated. Based on the results of this study, the following conclusions are drawn:

- The selective layer on the rGO/PAN composite membranes predominantly has small, similar-sized pores (~150 nm).
- An increase in the nanoadditive amount (0.11%–0.83% w/w of rGO) in the composite membrane results in an increased membrane surface porosity (21.75%–36.57%).
- Increased surface porosity creates pore formations with a smaller size distribution.
- Pore size has a decisive influence on the separation ($R > 80\%$) and anti-fouling properties of the rGO/PAN composite membranes, allowing particles smaller than 150 nm to be effectively separated.
- rGO/PAN composite membranes can be utilized for the single-stage treatment of wastewater containing MPs.

References

[1] Plastics - The Facts 2019, An Analysis of European Plastics Production, Demand and Waste Data, 2019. Available at: https://www.plasticseurope.org/en/resources/market-data

[2] R.C. Thompson, C.J. Moore, F.S.V. Saal, S.H. Swan, Plastics, the environment and human health: current consensus and future trends, Philos. Trans. R. Soc. B. Biol. Sci., 364 (2009) 2153–2166.

[3] R.C. Thompson, Y. Olsen, R.P. Mitchell, A. Davis, S.J. Rowland, A.W.G. John, D. McGonigle, A.E. Russell, Lost at sea: where is all the plastic?, Science, 304 (2004) 838–845.

[4] T. Poerio, E. Piacentini, R. Mazzei, Membrane processes for microplastic removal, Molecules, 24 (2019) 4148, doi: 10.3390/molecules24224148.

[5] J. Talvitie, A. Mikola, O. Setälä, M. Heinonen, A. Koistinen, How well is microlitter purified from wastewater? – A detailed study on the stepwise removal of microlitter in a tertiary level wastewater treatment plant, Water Res., 109 (2017) 164–172.

[6] M. Lares, M.C. Ncibi, M. Sillanpää, M. Sillanpää, Occurrence, identification and removal of microplastic particles and fibers in conventional activated sludge process and advanced MBR technology, Water Res., 133 (2018) 236–246.

[7] P. Liu, L. Qian, H. Wang, X. Zhan, K. Lu, C. Gu, S. Gao, New insights into the aging behavior of microplastics accelerated by advanced oxidation processes, Environ. Sci. Technol., 53 (2019) 3579–3588.

[8] J.P. Da Costa, A.R. Nunes, P.S.M. Santos, A.V. Girão, A.C. Duarte, T. Rocha-Santos, Degradation of polyethylene microplastics in seawater: insights into the environmental degradation of polymers, J. Environ. Sci. Health., Part A, 53 (2018) 866–875.

[9] V.M. Pathak, Navneet, Review on the current status of polymer degradation: a microbial approach, Bioresour. Bioprocess., 4 (2017) 15, doi: 10.1186/s40643-017-0145-9.

[10] T.S. Tofa, K.L. Kunjali, S. Paul, J. Dutta, Visible light photocatalytic degradation of microplastic residues with zinc oxide nanorods, Environ. Chem. Lett., 17 (2019) 1341–1346.

[11] G. Wang, L. Zhang, Y. Li, W. Zhao, A. Kuang, Y. Li, L. Xia, Y. Li, S. Xiao, Biaxial strain tunable photocatalytic properties of 2D ZnO/GeC heterostructure, J. Phys. D: Appl. Phys., 53 (2020) 1:015104, doi: 10.1088/1361-6463/ab440e.

[12] M.C. Ariza-Tarazona, J.F. Villarreal-Chiu, V. Barbieri, C. Siligardi, E.I. Cedillo-González, New strategy for microplastic degradation: green photocatalysis using a protein-based porous N-TiO_2 semiconductor, Ceram. Int., 45 (2019) 9618–9624.

[13] W. Perren, A. Wojtasik, Q. Cai, Removal of microbeads from wastewater using electrocoagulation, ACS Omega, 3 (2018) 3357–3364.

[14] B. Ma, W. Xue, Y. Ding, C. Hu, H. Liu, J. Qu, Removal characteristics of microplastics by Fe-based coagulants during drinking water treatment, J. Environ. Sci., 78 (2019) 267–275.

[15] B. Ma, W. Xue, C. Hu, H. Liu, J. Qu, L. Li, Characteristics of microplastic removal via coagulation and ultrafiltration during drinking water treatment, Chem. Eng. J., 359 (2019) 159–167.

[16] M. Enfrin, L.F. Dumée, J. Lee, Nano/microplastics in water and wastewater treatment processes – origin, impact and potential solutions, Water Res., 161 (2019) 621–638.

[17] J. Ma, Z. Wang, Y. Xu, Q. Wang, Z. Wu, A. Grasmick, Organic matter recovery from municipal wastewater by using dynamic membrane separation process, Chem. Eng. J., 219 (2013) 190–199.

[18] S. Ziajahromi, P.A. Neale, L. Rintoul, F.D.L. Leusch, Wastewater treatment plants as a pathway for microplastics: development of a new approach to sample wastewater-based microplastics, Water Res., 112 (2017) 93–99.

[19] L. Li, D. Liu, K. Song, Y. Zhou, Performance evaluation of MBR in treating microplastics polyvinylchloride contaminated polluted surface water, Mar. Pollut. Bull., 150 (2020) 1–6.

[20] M. Enfrin, J. Lee, P. Le-Clech, L.F. Dumée, Kinetic and mechanistic aspects of ultrafiltration membrane fouling by nano- and microplastics, J. Membr. Sci., 601 (2020) 117890, doi: 10.1016/j.memsci.2020.117890.
[21] B. Fryczkowska, A. Machnicka, D. Biniaś, C. Ślusarczyk, J. Fabia, The influence of graphene addition on the properties of composite rGO/PAN membranes and their potential application for water disinfection, Membranes, 10 (2020) 58, doi: 10.3390/membranes10040058.
[22] W.S. Hummers, R.E. Offeman, Preparation of graphitic oxide, J. Am. Chem. Soc., 80 (1958) 1339–1339.
[23] P. Pradyot, Handbook of Inorganic Chemicals, McGraw-Hill, New York, NY, 2003, p. 430.
[24] R.T. Bray, K. Fitobór, Sizes of iron hydroxide particles formed during ferric coagulation processes, Desal. Water Treat., 64 (2017) 419–424.
[25] R.R. Salunkhe, Y.V. Kaneti, Y. Yamauchi, Metal-organic framework-derived nanoporous metal oxides toward supercapacitor applications: progress and prospects, ACS Nano, 11 (2017) 5293–5308.